Available online at www.sciencedirect.com
ScienceDirect
Trans. Nonferrous Met. Soc. China 27(2017) 91−101
Transactions of Nonferrous Metals Society of China
www.tnmsc.cn

Stitch welding of Ti−6Al−4V titanium alloy by fiber laser

Cui LI[1], Bin LI[2], Ze-feng WU[1], Xiao-yong QI[1], Bing YE[1], Ai-hua WANG[1,2]

1. Hubei Provincial Key Laboratory of Laser Advanced Manufacturing Technology, Wuhan Huagong Laser Engineering Co., Ltd., Wuhan 430223, China;
2. School of Mechanical Science and Engineering, Huazhong University of Science and Technology, Wuhan 430074, China

Received 15 December 2015; accepted 17 August 2016

Abstract: Stitch welding of plate covered skeleton structure of Ti−6Al−4V titanium alloys has a variety of applications in aerospace vehicle manufacture. The laser stitch welding of Ti−6Al−4V titanium alloys was carried out by a 4 kW ROFIN fiber laser. Influences of laser welding parameters on the macroscopic geometry, porosity, microstructure and mechanical properties of the stitch welded seams were investigated by digital microscope, optical microscope, scanning electron microscope and universal tensile testing machine. The results showed that the three-pipe nozzle with gas flow rate larger than 5 L/min could avoid oxidization, presenting better shielding effect in comparison with the single-pipe nozzle. Porosity formation could be suppressed with the gap between plate and skeleton less than 0.1 mm, while the existing porosity can be reduced with remelting. The maximum shear strength of stitch welding joint with minimal porosity was obtained by employing laser power of 1700 W, welding speed of 1.5 m/min and defocusing distance of +8 mm.

Key words: Ti−6Al−4V titanium alloy; fiber laser; stitch welding; welding parameter; porosity

1 Introduction

Due to their high specific strength, excellent corrosion and high temperature resistance, titanium alloys have been recently used in the aerospace, automotive, medical devices and also military industries [1−3]. Conventional welding procedures can be used for joining Ti−6Al−4V sheets, but the lower material thermal conductivity and the stress produced by large heat input during welding usually lead to deformation of workpiece [4]. Nevertheless, laser welding presents particular suitability for welding of Ti−6Al−4V due to its high energy concentration, easy to realize automation and rapid processing capability [5]. A comparative study of gas tungsten arc welding, laser welding and electron beam welding of Ti−6Al−4V alloy has been researched by BALASUBRAMANIAN et al [6]. It has been reported that laser welds possess the narrowest fusion zone and heat affect zone.

For laser welding, parameters such as welding speed, output energy and focal position, directly influence the quality of welding joints. It is possible to control the penetration depth and geometry of the laser butt weld bead by precisely controlling the laser output parameters [7]. LIU et al [8] examined the joint strength of titanium using several levels of laser output energy. Due to the high rate of laser beam absorption and low thermal conductivity of titanium, a greater penetration depth has been obtained with increasing the output energy, under suitable condition, joint strength similar to that of parent metal could be achieved. CAO and JAHAZI [9] investigated the effects of laser welding speed on butt joint morphology and mechanical properties of Ti−6Al−4V. The result shows that the fusion zone area and underfill depth decrease with increasing welding speed, joints without or with minor defects can be obtained, and weldments have slightly higher joint strength but lower ductility compared with parent metal. Previous research has come to similar conclusions by WANG et al [10].

Since titanium is highly reactive with nitrogen, oxygen and hydrogen at high temperature, leading to lattice distortion or cracks in welds, gas shielding is very important for the titanium alloys in laser welding [7]. Usually, shielding gas such as argon or helium is brought

Foundation item: Project (2012BAF08B02) supported by Key Project in the National Science and Technology Pillar Program During the Twelfth Five-year Plan Period, China
Corresponding author: Bin LI; Tel: +86-27-87180405; Fax: +86-27-87180487; E-mail: licui0211@163.com; lismile615@163.com
DOI: 10.1016/S1003-6326(17)60010-4

in by means of a steel tube to the impact zone. The simulation results indicated that the assist gas rate should be larger than 7.5 L/min [11]. COSTA et al [12] have shown that, the Ti−6Al−4V weld beads are free of oxides when argon is used as shielding gas at a flow rate of 13 L/min. Meanwhile, the shielding gas can effectively avoid welding plume formation and then improve the keyhole stability [13]. However, the shielding gas in the molten pool that cannot escape before solidification will form porosity [14].

Up to now, a lot of investigations on laser welding of Ti−6Al−4V alloy have mainly concentrated on butt welding method, and laser stitch welding of Ti−6Al−4V alloy has been seldom reported. However, stitch welding joints of Ti−6Al−4V alloy have a variety of applications in aerospace vehicle manufacture, and the welding joints properties are closely associated with the machine's performance. In our work, Ti−6Al−4V plate and skeleton sheets with thickness of 1.6 and 6 mm were stitch welded by fiber laser welding. In order to get good quality of Ti−6Al−4V stitch welded joints, the effects of laser welding parameters (gas protection method, gas flow rate, laser power (P), welding speed (v), defocus distance (f), remelting times and gap between plate and skeleton) on welded seam morphology, porosity, microstructure and mechanical properties were investigated systematically.

2 Experimental

The annealed plates of the as-cast ZTC4 titanium alloy (105 mm × 15 mm × 6 mm) and TC4 titanium alloy (100 mm × 80 mm × 1.6 mm) were selected separately as skeleton and plate materials and their chemical compositions were shown in Table 1. A high-power (4 kW) ROFIN fiber laser equipped with YW52 laser and ABB IRB 4600 six-axis robot were employed. A collimation lens, a focal lens and an optical fiber were used to produce a focal spot of approximately 0.4 mm.

Table 1 Chemical compositions of titanium alloy (mass fraction, %)

Material	Al	Fe	Mo	V	C	Ti
TC4	5.18	4.16	0.026	4.01	≤0.10	Bal.
ZTC4	3.87	5.57	0.029	3.97	≤0.10	Bal.

To avoid reaction between the molten metal and the atmospheric moisture and oxygen, the welded seams were carefully shielded with pure argon gas. Two kinds of welding covering gas nozzles were designed, as shown in Fig. 1. One consisted of a single pipe (see Fig. 1(a)) and the other was combined with three pipes (see Fig. 1(b)). The first pipe was mainly to provide gas to prevent joint oxidation and eliminate the influence of plasma shielding during the welding process, while the other two were mainly to prevent weld oxidation during the process of welding and cooling. Both of the two nozzles were 2 mm away from the surface of plate, and the angle between blowing direction and welding direction was 135°.

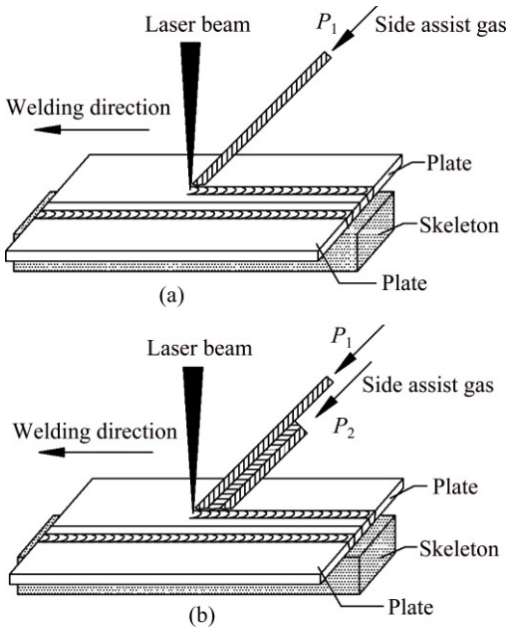

Fig. 1 Schematic diagrams of covering gas nozzles: (a) Single-pipe nozzle; (b) Three-pipe nozzle

In order to wipe off oxidation film and contamination, the surfaces of the plates were polished and cleaned with acetone prior to the clamping in weldment setup. Welding parameters such as gas protection method, gas flow rate, laser power, welding speed, defocusing distance, the gap between plate and skeleton and remelting times were investigated in this study to evaluate the effects on welding quality of lap joints.

For each welding condition, at least three weld cross-sections with four geometric parameters which had a great effect on the quality of the laser welding were analyzed to obtain weld dimensions, as shown in Fig. 2, where B represents the width of weld pool, b represents the connect width between plates, H represents the penetration depth of the welding and a represents the gap between plate and skeleton.

The quality of welded joints could be judged by the color of welded seam after welding. Welded seam with

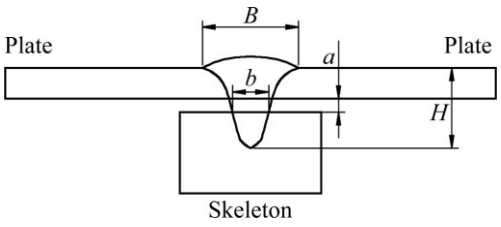

Fig. 2 Scheme of laser-welded cross section

shining color indicated the lowest pollution level [9]. The pore size and quantity were measured by longitudinal cross-section using digital microscope, as shown in Fig. 3. About 80 mm longitudinal cross-section was sampled in the middle of the longitudinal weld. The microstructures of the joint were observed by optical microscope (XJL−03). The shear strength of the joint at room temperature was evaluated with a universal tensile testing machine (WDW−200E) at a cross head speed of 2 mm/min with a load cell of 50 kN. The schematic diagram of the tensile specimen is shown in Fig. 4. To analyze broken position of the joints, the fracture surface of tensile specimens was characterized by a scanning electron microscope (JSM−5610LV).

Fig. 3 Typical longitudinal metallography of specimen

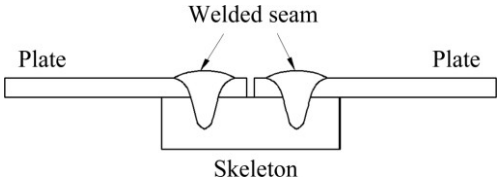

Fig. 4 Structure of tensile test sample

3 Results and discussion

3.1 Influence of process parameters on quality of welded seams

3.1.1 Gas nozzle type and gas flow rate

A set of experiments were designed by varying gas nozzle and gas flow rate between 1 L/min and 40 L/min, with other processing parameters kept constant, namely laser power P=1600 W, welding speed v=1.5 m/min and defocusing distance f=+4 mm. It can be seen that the flow rate of shielding gas has a great influence on the surface morphology, as shown in Fig. 5. The welded beads are oxidized obviously when the gas flow rate is lower than 5 L/min for the single-pipe nozzle and

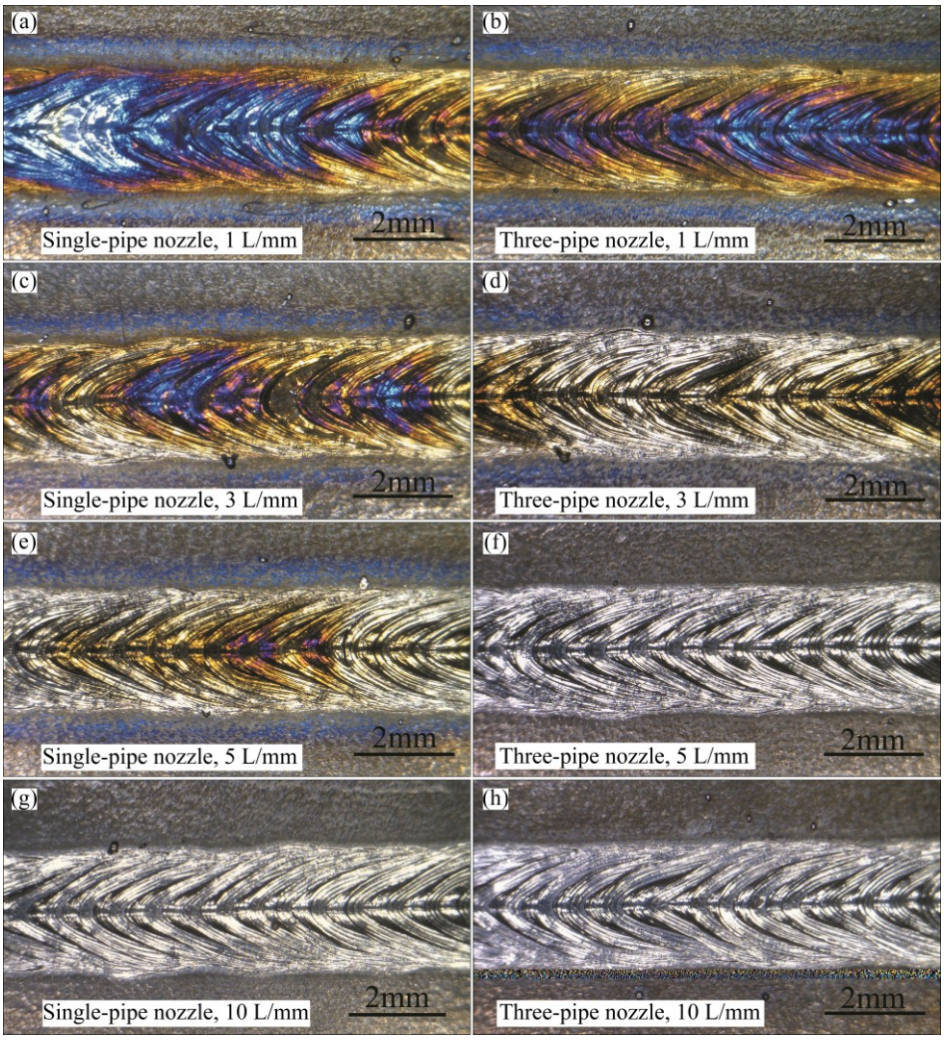

Fig. 5 Influences of gas nozzle type and gas flow rates on surface appearance of welded seams

3 L/min for the three-pipe nozzle. Silvery white color welded seams can be produced when the gas flow rate is larger than 10 L/min for the single-pipe nozzle or 5 L/min for the three-pipe nozzle.

There are two kinds of porosities in the welded seams, which are metallurgical porosity and characteristic porosity. The metallurgical porosity is characterized by spheroid shape with smooth inner wall and smaller diameter of 5−40 μm [15]. The characteristic porosity is irregular shape with larger sizes up to 80 μm [16]. Metallurgical porosity tends to locate near the fusion line, while characteristic porosity distributes mostly in the center of the welded seams, as shown in Figs. 6(a)−(d). The proportion of characteristic porosity area to welded cross-section area is 3.2%. There are more pores distributing in the upper plate than below one, as shown in Figs. 6(e) and (f).

The penetration depth and width of the welded seam have no significant change with the variation of gas flow rate, as shown in Fig. 7(a). The deeper penetration and narrower welded seams are produced by the three-pipe shielding gas nozzle rather than the single-pipe nozzle. Figure 7(b) shows the porosity number in variation with gas flow rate by two kinds of shielding gas nozzles. The porosity decreases when the shielding gas flow rate increases from 1 to 3 L/min. However, the porosity increases as the shielding gas flow rate increases continuously. The porosity number reaches the maximum value when the shielding gas flow rate is 20 L/min, which are 58 and 62 for single-pipe nozzle and the three-pipe nozzle, respectively. Then, the porosity starts to reduce again with increasing shielding gas flow rate.

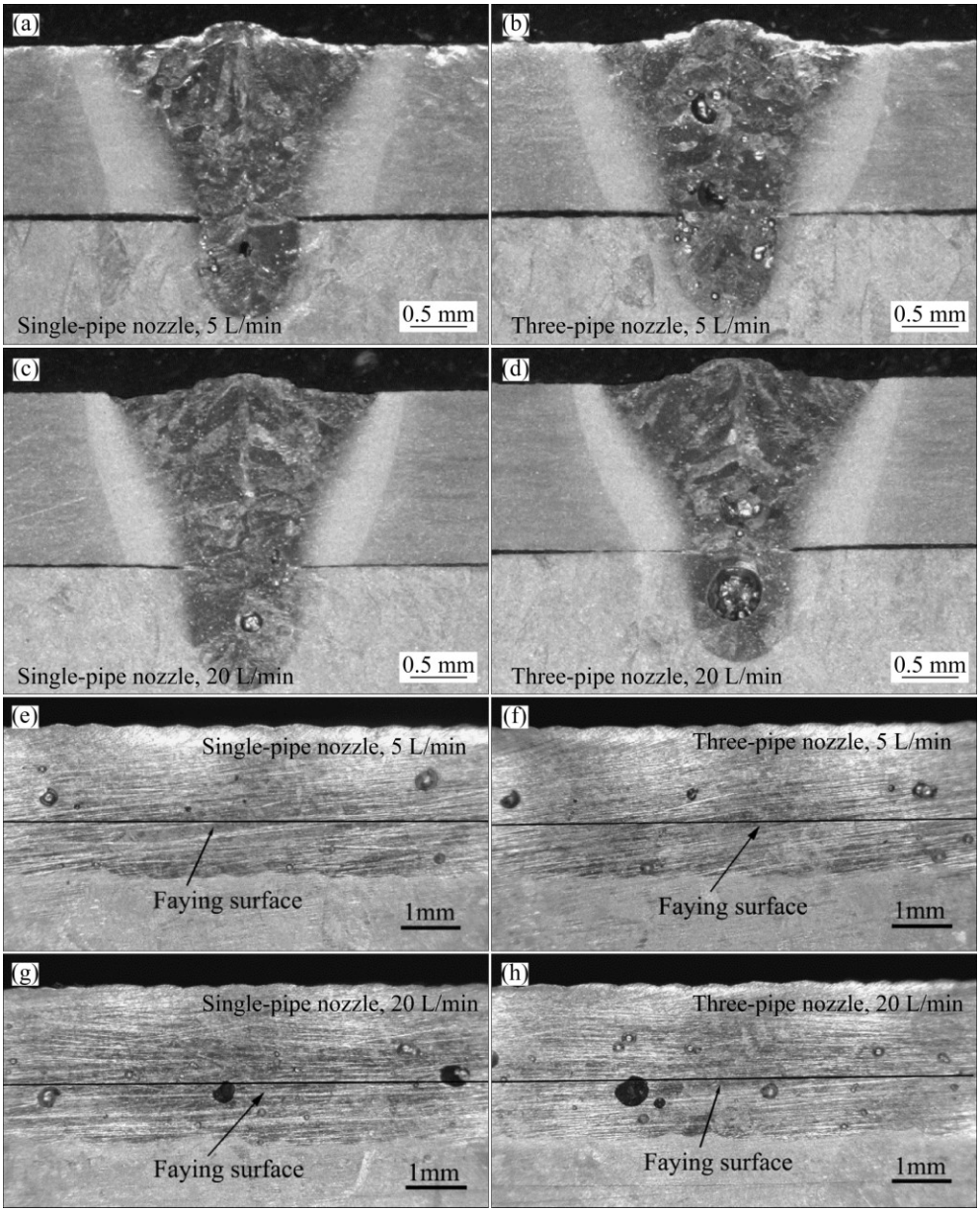

Fig. 6 Typical porosity distribution: (a−d) Cross section; (e−h) Longitudinal direction

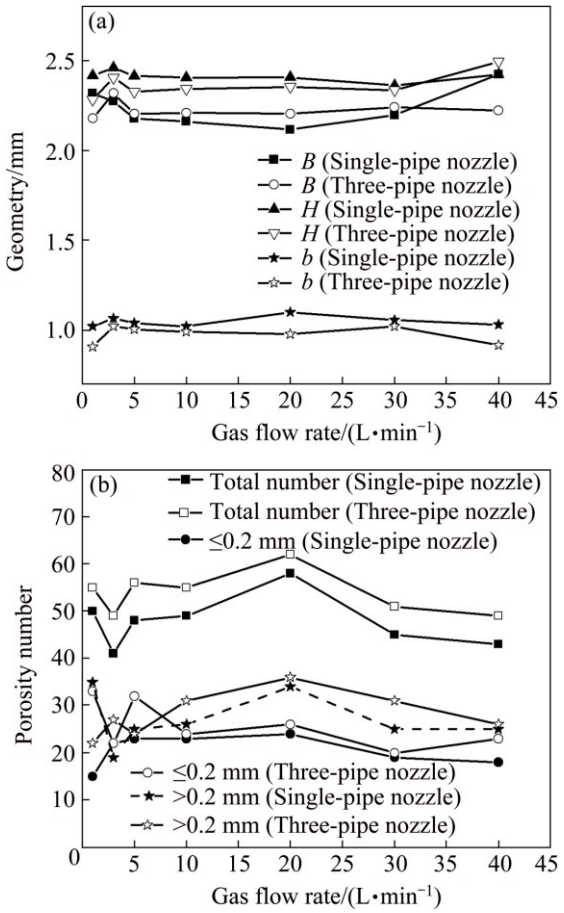

Fig. 7 Influences of gas flow rate on geometry (a) and porosity number (b)

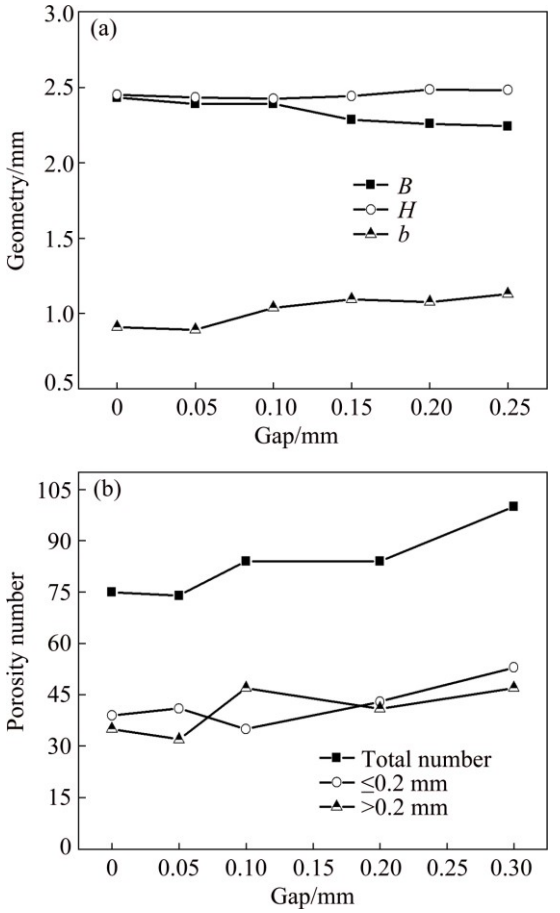

Fig. 8 Influences of gap between plate and skeleton on geometry (a) and porosity number (b) (Laser parameters: three-pipe nozzle, gas flow rate 5 L/min, P=1700 W, v= 1.5 m/min, f=+4 mm)

If gas flow rates keep the same(<10 L/min), the effective shielding zone of three-pipe nozzle is larger than that of single-pipe nozzle. When gas flow rate is sufficient, the optimized gas flow rate is above 30 L/min to restrain the occurrence opportunity of porosity.

3.1.2 Gap between plate and skeleton

The weld penetration and melting width change slightly when the gap between plate and skeleton is less than 0.1 mm, while the weld penetration decreases when the gap between plate and skeleton is larger than 0.1 mm, as shown in Fig. 8(a). An increase of gap between plate and skeleton results in the rising of porosity number significantly, as shown in Fig. 8(b). And the gap between the plate and skeleton less than 0.1 mm produces minimum porosity number of about 75, which is considered to be the optimal gap between plate and skeleton.

3.1.3 Laser power, welding speed and defocusing distance

Both penetration depth and melting width increase with increasing laser power or decreasing welding speed, as shown in Fig. 9, mainly due to the heat input per unit time is improved. The penetration depth increases not so obviously as melting width when the welding speed is less than 1.8 m/min. That is mainly because sustaining keyhole is the recoil pressure of metal vapor, the recoil pressure is not strong enough to maintain the existence of keyhole when the welding speed decreases to a certain extent, and that the keyhole would no longer deepen. The ratio of weld depth to width reaches the lowest level (0.94) and the maximum value (1.07) at the laser powers of 1500 and 2100 W, respectively. The ratio of weld depth to width reaches the lowest level (0.88) and the maximum value (1.17) at the welding speeds of 1.2 m/min and 1.8 m/min, respectively. Figures 9(c) and (d) illustrate the influences of laser power and welding speed on porosity number in the welded seams respectively. The quantity of porosity has a tendency to increase with the increase of either laser power or welding speed.

The influence of defocusing distance on the geometry of welded seam and porosity number is shown in Fig. 10. The laser power density inside the specimen is higher than that of the surface, and a deeper penetration can be obtained by using the negative defocusing distance. With the increase of defocusing distance, both

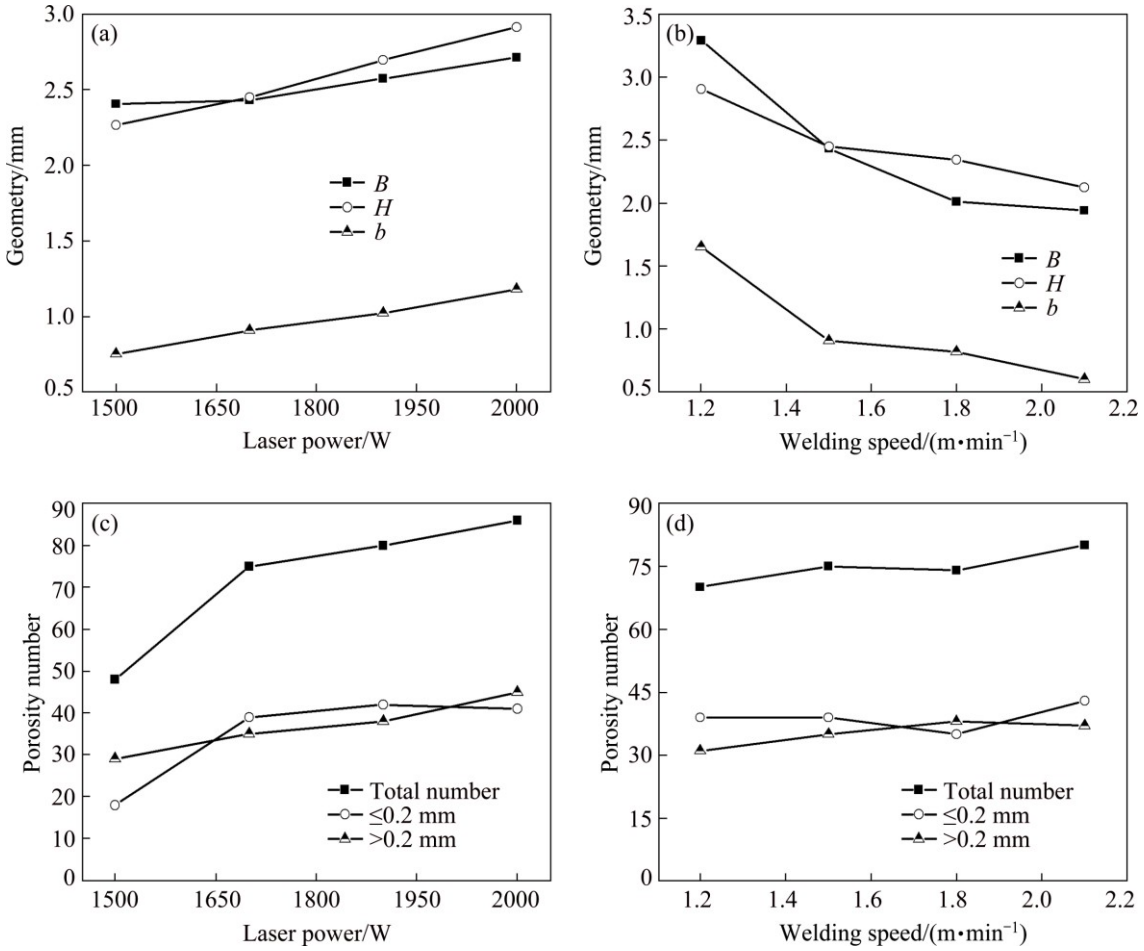

Fig. 9 Influences of laser power on geometry (a) and porosity number (c), and welding speed on geometry (b) and porosity number (d) (Laser parameters: three-pipe nozzle, gas flow rate 5 L/min, f = +4 mm) at v = 1.5 m/min (a, c) and P = 1700 W (b, d)

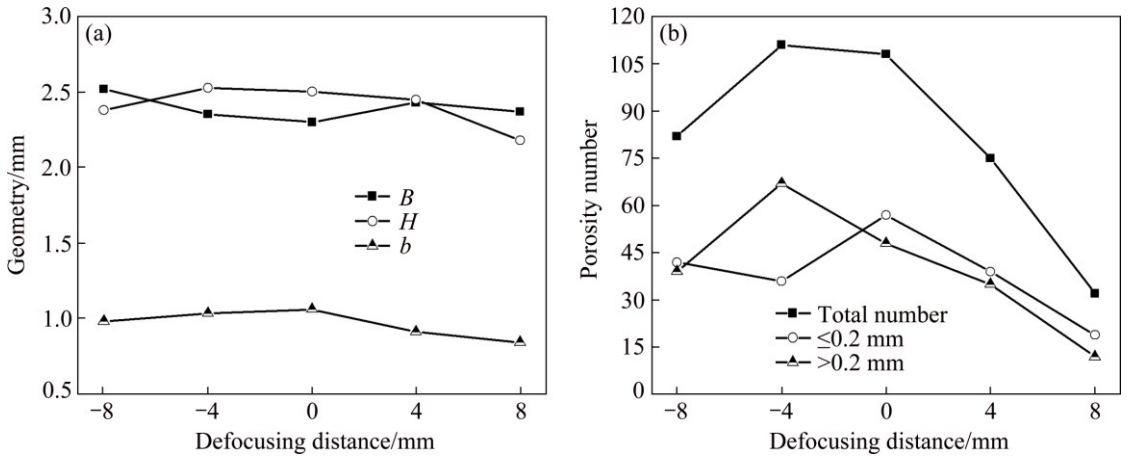

Fig. 10 Influences of defocusing distance on geometry (a) and porosity number (b) (Laser parameters: three-pipe nozzle, gas flow rate 5 L/min, P=1700 W, v = 1.5 m/min)

the width and penetration on the combined surface increase, while the weld width decreases. In the positive defocusing zone, the weld width increases, while both the width and penetration on the combined surface decrease, and it is smaller than the negative defocus. With the increase of defocusing distance, the total number of pores increases firstly and then decreases. Positive defocus decreases the number of pores. So, under the guarantee of penetration depth, it is better to take positive defocus to improve the quality of the welded joint.

3.1.4 Remelting times

The remelting times has no obvious influence on weld penetration and melting width (see Fig. 11);

however, the connection width between plates increases with increasing remelting times. Remelting can effectively decrease the porosity number that has already existed in the workpiece, especially taking more remelting times, but it has little effect on further reducing porosity when the remelting times is over twice. Therefore, in practical engineering applications, the remelting times should be better controlled at 1 or 2 to sufficiently use unqualified weld workpiece with excessive amount of porosity defects.

3.2 Microstructure

The microstructure of the TC4 alloy consists of two phases: α phase (HCP, hexagonal close-packed) and β phase (BCC, body-cantered cubic), and α+β phase exists in the form of equiaxed grains. β phase (black) distributes at the boundaries of α phase (white), as shown in Fig. 12(a). The microstructure of the ZTC4 alloy is a typical widmanstatten structure. This structure consists of thick flat α lamellae and β grain boundaries, as shown in Fig. 12(b). The α lamellae exists as bundling and alternating arrangement. Each β grain is composed of a number of α clusters which are separated by β lamella.

The microstructure of fusion zone (FZ) consists of a mixture of acicular martensitic α' phase, having a "basket-weave" distribution, as magnified in Figs. 12(c) and (d). The microstructure evolution of this zone is as follows. During the solidification stage, β grains grow in

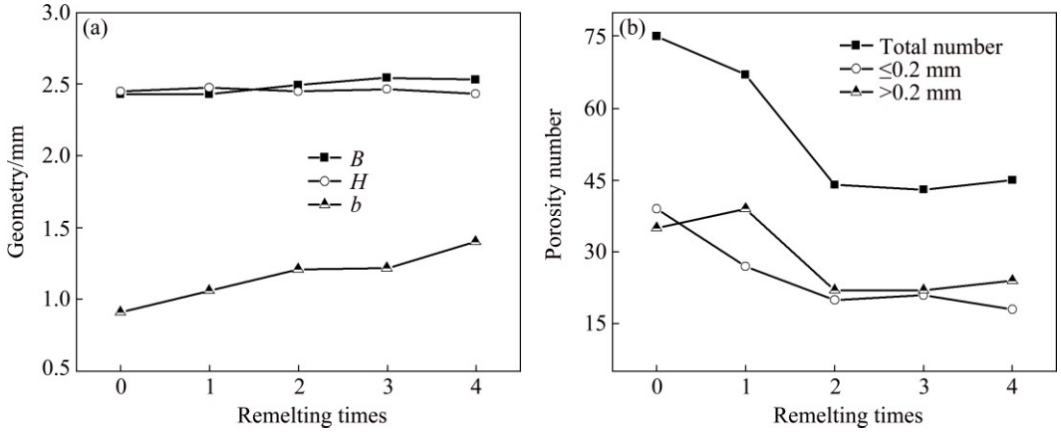

Fig. 11 Influences of remelting times on geometry (a) and porosity number (b) (Laser parameters: three-pipe nozzle, gas flow rate 5 L/min, P=1700 W, v=1.5 m/min，f=+4 mm)

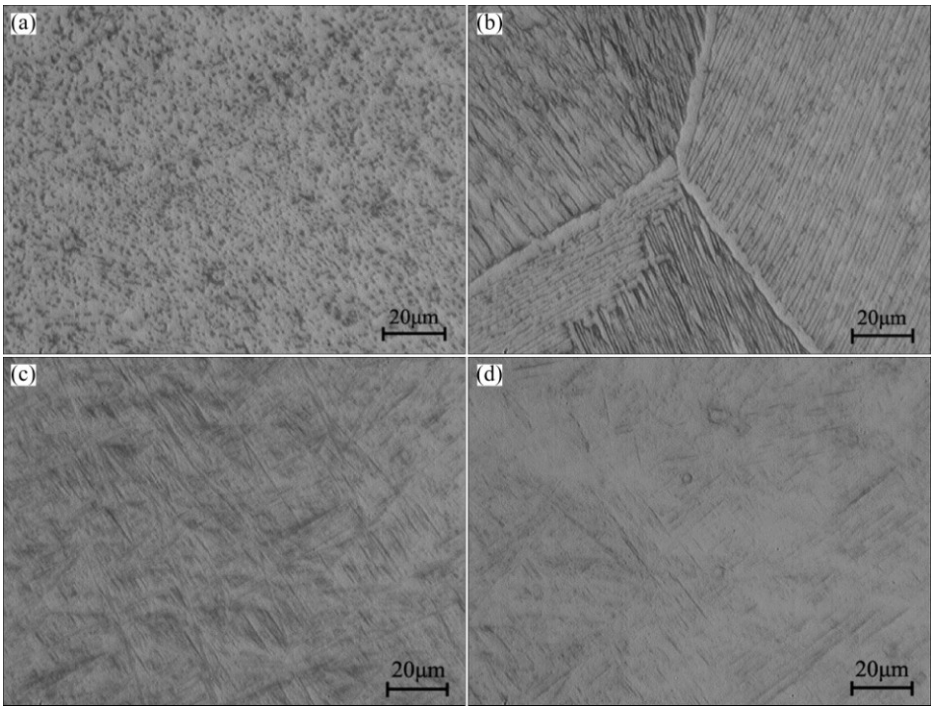

Fig. 12 Microstructures of TC4 parent metal of envelop material (a), ZTC4 parent metal of framework material (b), fusion zone adjacent to TC4 parent metal (c) and fusion zone adjacent to ZTC4 parent metal (d) (Laser parameters: three-pipe nozzle, gas flow rate 5 L/min, P=1700 W, v=1.5 m/min，f=+4 mm)

the direction of the heat flow. Due to the fast enough cooling rate, alloy elements are too slow to diffuse, so that no α structure develops from the prior β grain when the temperature reaches the β transus (980 °C). α' acicular martensite is formed with the emergence of diffusionless transformation (β turning into α' structure). Lots of parallel and primarily acicular α' martensites extend throughout the entire grain and stop at boundary of β grains. Then, a series of smaller α' grains start to precipitate. They stop growing up when they arrive at the other α' phase or grain boundaries. So, the classical basket-weave structure is formed. This martensite structure has not only good strength and hardness, but also better comprehensive performance, such as plastic, creep resistance and high endurance strength. Naturally, it is very difficult to discriminate different microstructures of the constituent morphology from a metallurgical analysis just based on optical microscopy over such a small area as the fusion zone. The sizes of the columnar grains are related to the microstructure of parent metal. Therefore, the size of α' acicular martensitic grains in the fusion zone of ZTC4 is larger than that of grains in the fusion zone of TC4. The microstructures of the TC4 and ZTC4 joint are described in more detail elsewhere [17].

3.3 Shear strength and fracture behaviour

Shear strength tests were performed to evaluate the mechanical properties of the joint. The fracture was located in the welded seam. The results of shear test of stitch joint are shown in Table 2. It can be seen that more pores distribute in welded seam, and lower shear strength of stitch joint is obtained. The pores located at the interface of these two kinds of parent metals have greater influence on the strength compared with other pores.

Table 2 Parameters of room temperature shear test of laser stitch welded joint

Width/ mm	Connecting width between plates/mm	Quantity of porosity	Maximum force/ kN	Shear strength/ MPa
9.77	1.129	108	7.363	667.523
9.77	0.91	75	6.256	703.657
9.77	0.84	32	6.028	734.513

A mass of dimples appear in parent metal and the fracture zone of laser welded joint, respectively, as shown in Figs. 13(a) and (b). On average, the size of dimples in the fracture zone of lap joint is smaller, which illustrates that the laser welded joint has better plasticity compared with the parent metal. The foregoing microstructure of welded seam is mainly composed of dense and fine acicular martensite. The dense grain boundary can produce interfacial strengthening effects, leading to the increase of strength and the hardness of the FZ and the HAZ. These results show that the lap joint exhibits the characteristics of ductile fracture.

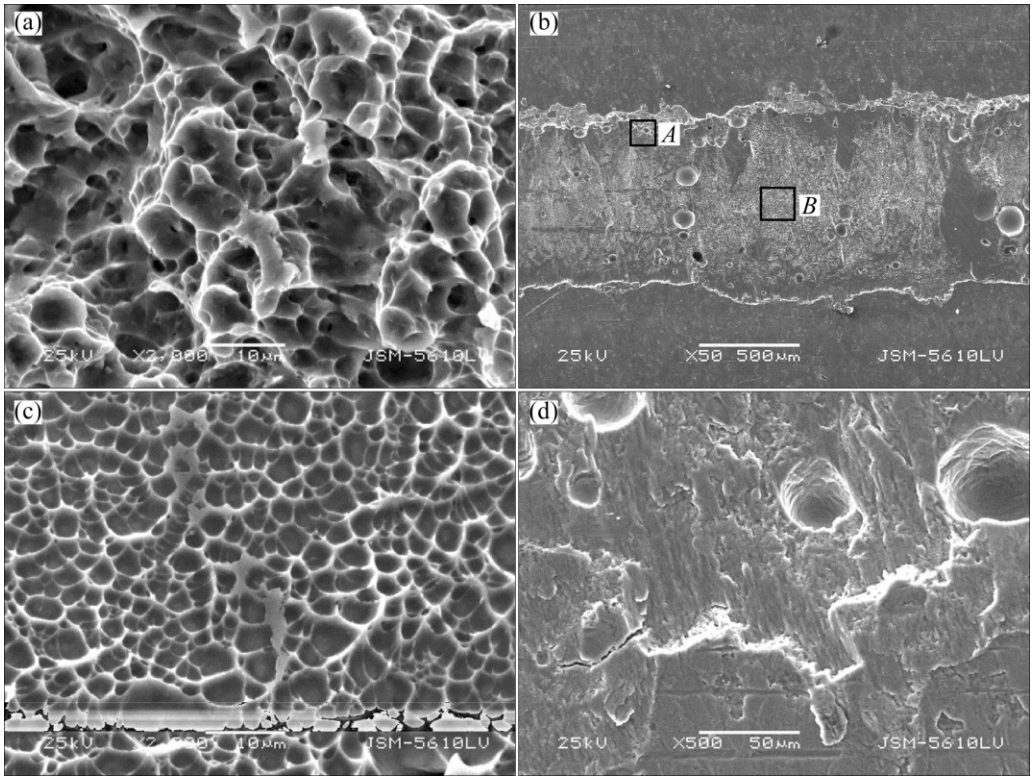

Fig. 13 SEM images of fracture surfaces: (a) Parent metal; (b) Welded seam; (c) Magnification of zone *A* from (b); (d) Magnification of zone *B* from (b)

The fracture initiates and propagates at the laser welded joint. Hence, the active area on the faying surface determines the shear resistance of joint directly. There are metallurgical porosity, craft porosity and cracks existing at the interface of plates, as shown in Figs. 13(c) and (d). A lot of characteristic pores distribute in the center of welded seam, while metallurgical pores locate in the margins of welded seam.

4 Discussion

4.1 Porosity formation mechanism for stitch welding of Ti−6Al−4V titanium alloys

Metallurgical porosity and characteristic porosity are two kinds of porosities generated in the laser welding process. The water absorbed from air, shielding gas and oxide film is the main reason for the forming of metallurgical porosity. Metallurgy pores tend to locate near the fusion line as the solubility of hydrogen in titanium decreases with temperature increasing, and large changes occur at solidification temperature point. Since the molten pool temperature in center area is higher than that of the edge and hydrogen is easily diffused from pool center to the edge, the pores are formed at weld pool edge where hydrogen is saturated. Metallurgical porosity distributes on the whole cross section of the welded seam and the small amount of metallurgical porosity has no significant effects on the mechanical properties of welded joint.

The characteristic porosity is attributed to the incorporation of gas such as argon and ambient air around the workpiece, which is mainly distributed in the center of FZ. Its forming is closely related to the fluctuation of keyhole, as shown in Fig. 14. Due to uneven absorption between hole of front wall and the laser energy, local convex exists in the front wall of hole. When the laser radiates at ridge, local metal will strongly evaporate, and liquid metal moves from top to bottom of the hole, leading to the close of hole. The pores are mainly occupied by metal vapor and gas involved, metal vapor will be deposited and attached to the pore wall along with molten pool solidification.

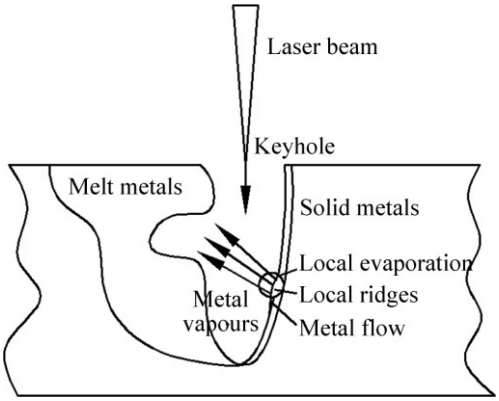

Fig. 14 Forming principle diagram of characteristic porosity

4.2 Effect of pores on shear strength

Shear strength of stitch welded joint decreases with the increase of porosity and crack defects. This is due to the formation of porosity in weld, directly reducing the effective stress area at the interface, i.e., directly reducing load area, and stress concentration coefficient of the defect, thus reducing the static load capacity as well. According to the principle of crack extension, it is easy to produce concentration in the weld defects in stressing situation. Therefore, the initiation and propagation of cracks generate from the defects, and the cracks cause the stress concentration in weld line, reducing fatigue properties and strength of the welded joint. This proves that porosity adversely affects the mechanical properties of the joint, and seriously affects the quality of welded joints. For the titanium alloy welded structure, the shear strength, fatigue resistance, corrosion resistance and fracture toughness are greatly reduced due to the pores distributing close to the fusion line and weld center. Therefore, reducing porosity in the weld by optimizing welding process parameters can improve the mechanical properties of stitch welded joint. It has important significance for ensuring the quality of products.

4.3 Effect of process parameters on porosity

The presence of this welding defect cannot be eliminated even though different welding parameters were adopted, but it could be reduced by optimizing parameters. When the gas flow rate was set to 1 L/min, molten pool was seriously oxidized, promoting the nucleation of hydrogen bubble, and more and more metallurgy porosities were formed in the welded seam. Welded seam was protected better with increasing shielding gas flow rate and the metallurgy porosity decreased. So, the total weld porosity number has a tendency to decrease with increasing gas flow rate. When the shielding gas flow rate was more than 3 L/min, the metallurgical porosity decreased but the gas pressure increased in welding molten pool. And the gas acting on the front wall of keyhole made local expansion, which resulted in the development of necking in other parts and the tendency of sharply rise of bubble formation. Thus, the characteristic porosity increased gradually. As a result, the total number of porosity increased. The protecting gas significantly eliminated the plasma when the flow rate increased to more than 20 L/min. Increasing gas flow rate also made the diameter of keyhole larger and more stable, which was in favor of decreasing porosity. Moreover, shielding gas caused a strong stirring effect, which led to uniform internal flow field in

welding pool that could contribute to gas leaking.

The porosity number increased with increasing the gap between plate and skeleton. The direction and frequency of molten pool flow changing with the gap between plate and skeleton increased and a small eddy was formed in the lower molten pool. Pores were formed at the bottom tip of keyhole during the welding. Since these bubbles were difficult to escape from the lower molten pool with large gap between plate and skeleton, the porosity was formed in welded beam. And the porosity number increased with increasing the gap between plate and skeleton [18]. Therefore, controlling the gap between plate and skeleton within 0.1 mm during laser stitch welding is a method to reduce or suppress porosity.

The width and depth of welded seam increased with the increase of laser power. When the welding speed is fast, the coagulation time of molten pool is short and the pore is easy to be formed since bubble is hard to escape from the molten pool. It was found that pores increased with increasing the laser power. This is because the depth of molten pool has a positive correlation with the laser power, and the bubble floating speed remains unchanged. Oppositely, bubbles escaped from molten pool need shorter time with the lower laser power and a shallower penetration depth.

The metal easily evaporated and the holes were formed when the power density of laser focus was very high. The porosity number tended to be the maximum when focal distance was zero. On the contrary, this tendency decreased when the focus point moved away from the surface of workpiece. The laser power density inside the specimen was higher than that of the surface under the negative defocusing distance. Therefore, the welded seam had more porosities with a negative defocusing distance than that with a positive defocusing distance.

Remelting can cut down porosities in the welded seam because there is not enough time for the gas to escape from molten pool for the rapid melting and solidification process of laser welding. However, the gas bubbles have a second chance to escape from welding seam by adopting remelting after welding.

5 Conclusions

1) The effective shielding zone of the three-pipe nozzle displays much better protection effect than that of the single-pipe nozzle at the same gas flow rate. Silver color welded seams could be obtained at the gas flow rates larger than 5 L/min by the three-pipe nozzle or 10 L/min by the single-pipe nozzle.

2) An increase in the gap between plate and skeleton results in large porosity number. The gap between plate and skeleton should be less than 0.1 mm, which is helpful for suppressing the porosity formation in welded seam.

3) A reduction of both laser power and welding speed, and positive defocusing distance can significantly suppress the porosity number in the welded seam.

4) Twice-remelting treatment could effectively decrease the porosity number. However, it has little effect on further reducing porosity number when the remelting times is more than 2.

5) The microstructure of the welded seam consists of two phases: α phase and β phase, and $\alpha+\beta$ phase exists in the form of equiaxed grains. Three types of defects in the stitch welded seam reduce the static load capacity of welded joints, and have a great influence on the shear strength of lap welded joint.

6) The maximum shear strength of TC4 plate and skeleton stitch welding joint can be obtained with minimal porosity by employing the optimal laser parameters: laser power 1700 W, welding speed 1.5 m/min and defocusing distance +8 mm.

References

[1] SCHUBERT E, KLASSEN M, ZERNER I, WALZ C, SEPOLD G. Light-weight structures produced by laser beam joining for future applications in automobile and aerospace industry [J]. Journal of Materials Processing Technology, 2001, 115(1): 2−8.

[2] ZHANG Bing-gang, SHI Ming-xiao, CHEN Guo-qing, FENG Ji-cai. Microstructure and defect of titanium alloy electron beam deep penetration welded joint [J]. Transactions of Nonferrous Metals Society of China, 2012, 22(11): 2633−2637.

[3] XU Pei-quan. Microstructure characterization of Ti−6Al−4V titanium laser weld and its deformation [J]. Transactions of Nonferrous Metals Society of China, 2012, 22(9): 2118−2123.

[4] GAO Xiao-long, ZHANG Lin-jie, LIU Jing, ZHANG Jian-xun. A comparative study of pulsed Nd: YAG laser welding and TIG welding of thin Ti6Al4V titanium alloy plate [J]. Materials Science and Engineering A, 2013, 559(3): 14−21.

[5] LI Z, GOBBI S L, NORRIS I, ZOLOTOVSKY S, RICHTER K H. Laser welding techniques for titanium alloy sheet [J]. Journal of Materials Processing Technology, 1997, 65(1−3): 203−208.

[6] BALASUBRAMANIAN T S, BALAKRISHNAN M, BALASUBRAMANIAN V, MANICKAM M A M. Influence of welding processes on microstructure, tensile and impact properties of Ti−6Al−4V alloy joints [J]. Transactions of Nonferrous Metals Society of China, 2011, 21(6): 1253−1262.

[7] AKMAN E, DEMIR A, CANEL T, SINMAZÇELIK T. Laser welding of Ti6Al4V titanium alloys [J]. Journal of Materials Processing Technology, 2009, 209(8): 3705−3713.

[8] LIU J, WATANABE I, YOSHIDA K, ATSUTA M. Joint strength of laser-welded titanium [J]. Dental Materials, 2002, 18(2): 143−148.

[9] CAO X, JAHAZI M. Effect of welding speed on butt joint quality of Ti−6Al−4V alloy welded using a high-power Nd: YAG laser [J]. Optics and Lasers in Engineering, 2009, 47(11): 1231−1241.

[10] WANG S H, WEI M D, TSAY L W. Tensile properties of LBW welds in Ti−6Al−4V alloy at evaluated temperatures below 450 °C [J]. Materials Letters, 2003, 57(12): 1815−1823.

[11] WANG Hong, SHI Yao-wu, GONG Shui-li, DUAN Ai-qin. Effect of assist gas flow on the gas shielding during laser deep penetration

welding [J]. Journal of Materials Processing Technology, 2007, 184(1−3): 379−385.
[12] COSTA A, MIRANDA R, QUINTINO L, YAPP D. Analysis of beam material interaction in welding of titanium with fiber lasers [J]. Materials and Manufacturing Processes, 2007, 22(7): 798−803.
[13] SCHNEIDER A, GUMENYUK A, LAMMERS M, MALLETSCHEK A, RETHMEIER M. Laser beam welding of thick titanium sheets in the field of marine technology [J]. Physics Procedia, 2014, 56: 582−590.
[14] GAO Xiao-long, ZHANG Lin-jie, LIU Jing, ZHANG Jian-xun. Porosity and microstructure in pulsed Nd: YAG laser welded Ti6Al4V sheet [J]. Journal of Materials Processing Technology, 2014, 214(7): 1316−1325.
[15] YU Yang-chun, WANG Chun-ming, HU Xi-yuan, WANG Jun, YU Sheng-fu. Porosity in fiber laser formation of 5A06 aluminum alloy [J]. Journal of Mechanical Science and Technology, 2010, 24(5): 1077−1082.
[16] MATSUNAWA A, MIZUTANI M, KATAYAMA S, STEO N. Porosity formation mechanism and its prevention in laser welding [J]. Welding International, 2003, 17(2): 431−437.
[17] WU Bing, LI Jin-wei, TANG Zhen-yun. Study on the electron beam welding process of ZTC4 titanium alloy [J]. Rare Metal Materials and Engineering, 2014, 43(4): 786−790.
[18] MENG W, LI Z G, LU F G, WU Y X, CHRN J H, KATAYAMA S. Porosity formation mechanism and its prevention in laser lap welding for T-joints [J]. Journal of Materials Processing Technology, 2014, 214(8): 1658−1664.

Ti−6Al−4V 钛合金光纤激光叠焊

李 翠[1]，李 斌[2]，吴泽锋[1]，祁小勇[1]，叶 兵[1]，王爱华[1,2]

1. 武汉华工激光工程有限责任公司 激光先进制造技术湖北省重点实验室，武汉 430223；
2. 华中科技大学 机械科学与工程学院，武汉 430074

摘 要：Ti−6Al−4V 钛合金蒙皮和骨架叠焊在航空航天器制造领域有着广泛应用。采用 4 kW ROFIN 光纤激光器对其进行激光叠焊，利用数码显微镜、光学显微镜、扫描电镜和万能试验机研究激光焊接工艺参数对叠焊焊缝几何尺寸、气孔数量、显微组织和力学性能的影响。结果表明，三管侧吹保护气嘴优于单管侧吹保护气嘴，气流量≥5 L/min 时可获得无氧化的焊缝；间隙控制在 0.1 mm 范围内能有效抑制气孔生成，重熔能有效地减少焊缝中已有的气孔；当激光焊接功率、焊接速度和离焦量分别为 1700 W、1.5 m/min 和+8 mm 时可制得气孔最少、剪切强度最高的叠焊接头。

关键词：Ti−6Al−4V 钛合金；光纤激光；叠焊；焊接参数；气孔

(Edited by Wei-ping CHEN)